

Spectral Efficiency of Low Earth Orbit Satellite Constellations

Cuneyd Ozturk, Dongning Guo, Randall A. Berry, and Michael L. Honig

Abstract—This paper investigates the maximum downlink spectral efficiency of low earth orbit (LEO) constellations. Spectral efficiency, in this context, refers to the sum rate of the entire network per unit spectrum per unit area on the earth's surface. For practicality all links employ single-user codebooks and treat interference as noise. To estimate the maximum achievable spectral efficiency, we propose and analyze a regular configuration, which deploys satellites and ground terminals in hexagonal lattices. Additionally, for wideband networks with arbitrary satellite configurations, we introduce a subband allocation algorithm aimed at maximizing the overall spectral efficiency. Simulation results indicate that the regular configuration is more efficient than random configurations. As the number of randomly placed satellites increases within an area, the subband allocation algorithm achieves a spectral efficiency that approaches the spectral efficiency achieved by the regular configuration. Further improvements are demonstrated by reconfiguring associations so that nearby transmitters avoid pointing to the same area.

Index Terms—Channel capacity, interference, spectrum allocation, low earth orbit (LEO) constellation, throughput.

I. INTRODUCTION

Satellite communications has experienced a surge of innovation, investment, and competition, with constellations of non-geostationary (NGSO) satellites in low earth orbits (LEO) emerging as a central focus. This trend can be attributed to advancements in satellite miniaturization, cost-effective launch technologies, and enhanced communication protocols [1]. In contrast to other satellite systems, LEO constellations offer notable advantages in terms of latency, data transfer rates, and coverage [2]–[4]. In the United States, so far more than twenty companies have pursued authorization from the Federal Communications Commission (FCC) to deploy more than 70,000 LEO satellites operating in Ku-/Ka-/V- bands [5], [6].

Analyzing the spectral efficiency of LEO constellations is important for several reasons. First, it allows an examination of the potential of LEO constellations for meeting global demand for reliable internet connectivity. Second, it provides insight into scalability and performance limitations that can guide network optimization and deployment strategies, enabling satellite service providers to make informed investment decisions. It also may provide insights useful for evolving satellite regulatory frameworks [6], [7].

We investigate the total downlink throughput that is achievable by a satellite constellation at a fixed altitude. A central figure of merit is the *spectral efficiency* in bits per second per Hz per square kilometers, which is defined as the total data rate

divided by the available bandwidth and Earth's surface area. In particular, we are interested in how the spectral efficiency depends on the density of the constellation. For practicality, we assume single-user codebooks and treat interference as independent additive white Gaussian noise (AWGN).

As the operator of a terrestrial cellular network densifies its network by deploying more access points, a user's distance to its nearest access point decreases. As a consequence, the total throughput can scale linearly with the number of access points in the interference-limited regime [8]. In contrast, the distance between a transmitter and its receiver in a satellite network cannot be less than the satellite's altitude, regardless of the density. Hence the denser the links, the stronger the aggregate interference is relative to the direct link. This suggests that the sum spectral efficiency of the satellite network is fundamentally limited.

To illustrate this point, we first evaluate the spectral efficiency of a stylized network with satellites forming a regular hexagonal lattice, where each satellite communicates with a unique ground terminal directly below it. For a single-channel network in which all satellites use the entire bandwidth, the spectral efficiency is bounded, and typically maximized at a unique density, or inter-satellite distance (see Fig. 4). That is, the spectral efficiency decreases as the density increases beyond a certain point due to excessive interference. The optimal density depends on the altitude, beamwidths (for both satellites and ground users), and signal-to-noise ratio (SNR).

Since the maximum spectral efficiency generally depends on the network topology, we ask: does the preceding regular topology of satellites and ground users maximize the downlink spectral efficiency in a single-channel network? We consider this question for satellite to ground user assignments that minimize the corresponding link distance. While it is difficult to prove a general optimality result, we show that orienting ground terminals directly below respective serving satellites maximizes received signal-to-interference-and-noise ratio (SINR), and observe numerically that the spectral efficiency of the regular configuration upper bounds the spectral efficiency associated with random placement of satellites and ground terminals.

With multiple subbands we show that characterization of the maximum spectral efficiency reduces to the single channel scenario by partitioning a network with multiple channels into single-channel sub-networks. Given a fixed satellite/ground user configuration with multiple subbands, we propose a subband allocation algorithm with a frequency reuse pattern to maximize the spectral efficiency. As network density increases, the spectral efficiency achieved by this algorithm for randomly placed satellite/ground user configurations approaches that of a regularly placed network.

Finally, we show that in the high density regime, minimum distance-association of satellites with ground terminals can be

C. Ozturk is with Aselsan Inc., Ankara, 06800, Turkey (E-mail: cuneydozturk@aselsan.com)

D. Guo, R. Berry and M. L. Honig are with the Department of Electrical and Computer Engineering, Northwestern University, Evanston, IL, 60208 USA (E-mails: dguo@northwestern.edu; rberry@northwestern.edu; mh@eeecs.northwestern.edu)

This work was supported in part by the NSF under Grant No. 1910168 and SpectrumX, an NSF Spectrum Innovation Center under Grant No. 2132700.

suboptimal. We give an example for a regular configuration in which assigning each satellite to a terminal outside a minimum-distance region improves the spectral efficiency by reducing interference. The key observation is that, if interfering satellites “look away” from a terminal that “looks toward” them, they cause substantially less interference.

Related work on evaluating the spectral efficiency of LEO constellations dates back at least to the era of the Iridium system. Ref. [9] explores the Iridium satellite constellation’s ability to support a certain number of ground terminals by modeling the network as a multi-hop communication system. In other work [10], the outage probability versus the minimum carrier-to-interference power ratio is examined for LEO, medium earth orbit, and geostationary orbit satellites across four distinct satellite constellations. Upper and lower bounds for the probability density of the number of successful beam assignments is derived in [11], and the impact of traffic non-uniformity on the signal-to-interference ratio (SIR) under hexagonal service assumptions for satellites is explored in [12].

Several authors have also evaluated the performance of satellite networks by modeling satellite and ground terminal location distributions as Poisson point process and variations [13]–[20]. Here our emphasis is on characterizing the spectral efficiency and resource management of LEO satellite constellations in the interference-limited regime.

The remainder of the paper is organized as follows. Sec. II describes the system model. Sec. III presents a particular regular configuration for satellites and ground terminals along with the spectral efficiency objective for a single-channel network. Sec. IV analyzes the spectral efficiency of the regular configuration for both narrowband and wideband scenarios. Sec. V addresses the channel allocation problem with an arbitrary configuration. Sec. VI discusses how changing link directions from nearest neighbor associations can increase the spectral efficiency. Sec. VII presents numerical results and concluding remarks are given in Sec. VIII.

II. SYSTEM MODEL

We consider the downlink of a LEO network of satellites transmitting to ground terminals. For simplicity we focus on single-hop satellite-ground station links, and ignore inter-satellite links and communications with gateways that may be used to enhance capacity and coverage. The downlink spectral efficiency (bits/s/Hz/km²) depends on many factors, including the number of satellites and ground terminals and their locations, transmission powers, beamwidths, main beam (look) directions, transmission schedules in time, frequency, as well as associations between satellites and ground users.

We analyze a model where ground terminals are distributed on a sphere representing the earth’s surface with radius $r_e = 6378$ km, and the satellites are distributed over a larger concentric sphere with radius $r_e + h$, where h (km) denotes the altitude of the satellites. Our goal is to characterize the maximum achievable spectral efficiency as a function of satellite and ground terminal beamwidths and satellite transmission power constraints. The results will also provide insight into the maximum throughput of large satellite (mega-)constellations. While we focus on downlink transmissions, a similar analysis can also be applied to the uplink.

A. Satellite-Ground Terminal Associations

We assume that each satellite can provide service to multiple ground terminals by utilizing multiple spot beams. We exclude the scenario where a ground terminal is being served by multiple satellites.

Let $F(\cdot)$ denote the association between the satellites and the ground terminals, i.e., ground terminal k is served by satellite $F(k)$. Also, satellite i serves the set of the ground terminals A_i so that $F(j) = i$ for $j \in A_i$. Hence satellite i controls $|A_i|$ independent spot beams where $|\cdot|$ is the cardinality of the set. In addition, $s_k \in \{1, \dots, |A_{F(k)}|\}$ denotes the serving spot beam index for terminal k . Received signals from other spot beams are treated as interference.

B. Time and Frequency Resources

We assume time slots, which are sufficiently short (e.g., milliseconds) so that the satellite configuration remains essentially constant over a time slot. Let \mathcal{B} denote the set of frequencies available for downlink satellite communication. In general, the set of available frequencies is a collection of M subbands or disjoint intervals denoted as $\mathcal{B}_1, \dots, \mathcal{B}_M$. Let their union be denoted by \mathcal{B} . Let $|B_m|$ denote the bandwidth of \mathcal{B}_m .

The set $S_i \subseteq \{1, \dots, M\}$ denotes the subband indices allocated to satellite i . Similarly, $G_k \subseteq \{1, \dots, M\}$ denotes the subband indices allocated to terminal k . The subbands allocated to terminal k must be a subset of the subbands allocated to satellite $F(k)$, i.e., $G_k \subseteq S_{F(k)}$.

Each satellite spot beam must satisfy two power constraints: Its total transmit power over \mathcal{B} cannot exceed P_{\max} , and its power spectral density (PSD) cannot exceed $\text{PSD}_{\max}(f)$ for any $f \in \mathcal{B}$, where $\text{PSD}_{\max}(f)$ is piece-wise smooth, i.e.,

$$\int_{\mathcal{B}} P_i^\ell(f) df \leq P_{\max} \quad (1)$$

and

$$P_i^\ell(f) \leq \text{PSD}_{\max}(f), \forall f \in \mathcal{B} \quad (2)$$

where $P_i^\ell(f)$ is the PSD of the ℓ^{th} spot beam for satellite i . Since the same power constraints apply to all time slots, it suffices to analyze the spectral efficiency of a single time slot. For purposes of obtaining an upper bound on spectral efficiency, we note that although a mega-constellation is constantly moving, the average spectral efficiency over time cannot exceed the spectral efficiency achieved when the mega-constellation is in its most favorable configuration. We also assume that Doppler shift is perfectly compensated at the terminals.

C. Propagation Model

The link gain between a satellite and a ground terminal is determined from the path-loss and antenna gains of the satellite and the ground user. At a given frequency f , the path-loss between satellite i and terminal k is modeled as $\psi_{i,k}(f)d_{i,k}^{-\alpha}$, where $\psi_{i,k}(f)$ ¹ and $d_{i,k}$ denote the frequency dependent gain and associated distance or link length, respectively, and $\alpha \geq 2$ denotes the path-loss exponent.

We assume that all satellite spot beams have the same (first-null) beam-width B_{sat} and the same antenna pattern $w_s(\cdot)$. All

¹For example, with Friis path loss $\psi_{i,k}(f) = (c/(4\pi f))^2$.

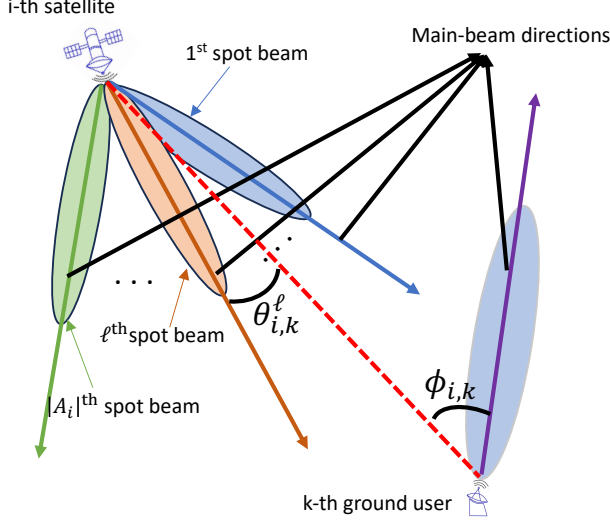


Fig. 1. Illustration of off-axis angles for the satellite spot beams and ground terminals.

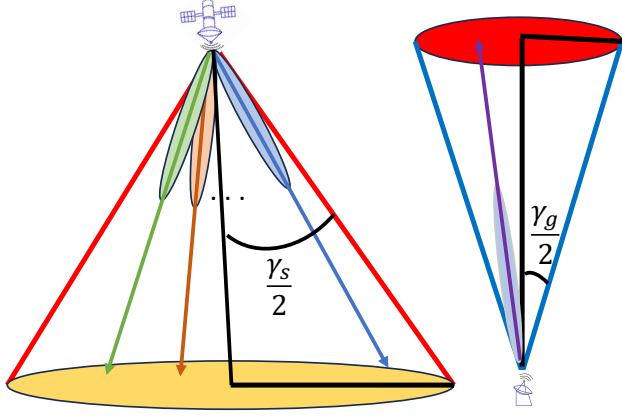


Fig. 2. Satellite and ground terminal main-beam (look) directions within the regions specified by γ_s and γ_g , respectively.

ground terminals have a single beam with the same (first-null) beam-width B_{gs} and the same antenna pattern $w_g(\cdot)$.

Referring to Fig. 1, let $\theta_{i,k}^\ell$ denote the off-axis angle between the main-beam direction of the ℓ^{th} spot beam for satellite i and the direction from satellite i to terminal k . Similarly, let $\phi_{i,k}$ denote the off-axis angle between the main-beam (receive) direction of terminal k and the direction from terminal k to satellite i . The link gain between the ℓ^{th} spot beam of satellite i and terminal k is²

$$\Omega_{i,k}^\ell(f) \triangleq \psi_{i,k}(f) d_{i,k}^{-\alpha} w_s(\theta_{i,k}^\ell) w_g(\phi_{i,k}). \quad (3)$$

The SINR at terminal k is then

$$\text{SINR}_k(f) = \frac{P_{F(k)}^{s_k}(f) \Omega_{F(k),k}^{s_k}(f)}{\sum_{(i,\ell) \neq (F(k), s_k)} P_i^\ell(f) \Omega_{i,k}^\ell(f) + N_0}, \quad (4)$$

where N_0 denotes the single-sided PSD of the AWGN (ad-

²We assume normalized beam-patterns, where G_{\max} , the product of the highest gains of the satellite and ground terminal beam-patterns, is included in $\psi_{i,k}(f)$, since all satellite spot beams have the same beam-pattern $w_s(\cdot)$ and all ground terminals have the same beam-pattern $w_g(\cdot)$.

ditive white Gaussian noise) at each terminal. The spectral efficiency objective for the satellite network is

$$R = \frac{1}{4\pi r_e^2 B} \sum_k \sum_{i \in G_k} \int_{B_i} \log_2(1 + \text{SINR}_k(f)) df. \quad (5)$$

We further assume that the main-beam direction of each satellite spot beam and receive beam direction for each ground terminal are constrained to point within regions defined by angles γ_s and γ_g as depicted in Fig. 2. We refer to these regions as the *beam regions* of the satellites and ground terminals.

D. Reduction to Single-Channel Network

To estimate the maximum spectral efficiency of a satellite network, we conduct an analysis assuming that the operator can deploy an unlimited number of satellites at arbitrary positions, with no restrictions on the number of ground terminals. Under this assumption, we shall show that the optimal spectral efficiency is achieved with a finite number of satellites and terminals, and it suffices to consider a single-channel network defined as follows:

- 1) All satellites and ground users use the same narrow subband;
- 2) Each satellite serves a unique ground user with a single-beam;
- 3) Each ground user is served by a unique satellite.

In particular, we argue that for any satellite network, there exists a single-channel satellite network whose spectral efficiency upper bounds that of the former network.

First, without limiting the number of ground terminals, we can replace terminal k with $|G_k|$ co-located terminals, each served by a different subband allocated to satellite $F(k)$. This operation does not affect (5). Applying this procedure to all terminals gives a network in which each terminal is served by a single subband.

Second, without limiting the number of satellites, we can replace satellite i with $|S_i| \times |A_i|$ satellites at the same position, each with a single spot beam assigned a single subband, and subject to the same power constraints (1) and (2). This is transparent to the receivers since their received signals do not change. Hence, as far as maximizing the spectral efficiency is concerned, it suffices to consider one dedicated ground terminal for each satellite.

The total data rate of a collection of single-hop links over a set of orthogonal subbands can be achieved by coding over them separately (assuming codelengths are not a limitation). Hence the problem of maximizing the spectral efficiency over the frequency resource \mathcal{B} can be divided into M different subproblems over $\mathcal{B}_1, \dots, \mathcal{B}_M$, respectively. In other words, if C_m upper bounds the spectral efficiency for the satellite-ground user links operating over \mathcal{B}_m , then the overall spectral efficiency will be upper bounded by $\sum_m C_m B_m / B$. It is evident that the total power constraint (1) becomes irrelevant as M becomes large, that is, the PSD constraint becomes binding.

III. SINGLE-CHANNEL MODEL

Given the preceding reduction to a single-channel network, in what follows we drop the spot beam index ℓ from both the PSD $P_i(f)$ and link gain $\Omega_{i,k}(f)$. Moreover, due to the narrowband assumption, we take the transmitted PSDs to be

constants, that is, $P_i(f) = p_i \leq \text{PSD}_{\max}(f) = \text{psd}_{\max}$ for each i , and all frequency dependent gains are assumed to be constant $\psi_{i,k}(f) = \psi_{i,k}$ for each i and k . In particular, $\psi_{i,k}(f) = \psi$ independent of i and k . Hence, the path loss for link $i \rightarrow k$ has the form $\Omega_{i,k}(f) = \Omega_{i,k} = d_{i,k}^{-\alpha} w_{i,k} \psi$, where $w_{i,k}$ is the product of the antenna gains at the satellites and the ground users. In what follows the satellite and the ground terminal locations are denoted as $(s_i)_{i=1}^N$ and $(g_k)_{k=1}^N$, respectively, where N is the total number of satellites.

A. Link Associations

For the single-channel network associations are one-to-one, i.e., F is a permutation of $\{1, \dots, N\}$. As a baseline, we first select the association to minimize

$$\sum_{k=1}^N \|s_{F(k)} - g_k\|^2 \quad (6)$$

where $\|\cdot\|$ denotes Euclidean norm (e.g., see [13], [14], [20]). The Hungarian algorithm [21] can be used to determine $F(\cdot)$. We then reassign the indices of the ground terminals so that $F(k) = k$.

B. Spectral Efficiency

Let \mathcal{I}_k denote the set of interfering satellites in the field of view for terminal k , all satellites except the serving satellite above the horizon for terminal k . Then the SINR at terminal k in (4) can be written as

$$\text{SINR}_k = \frac{p_k d_{k,k}^{-\alpha} w_{k,k}}{\sum_{i \in \mathcal{I}_k} p_i d_{i,k}^{-\alpha} w_{i,k} + \sigma^2}, \quad (7)$$

where $\sigma^2 = N_0/(2\psi)$. In this case, the objective in (5) becomes:

$$R = \frac{1}{4\pi r_e^2} \sum_{k=1}^N \log_2(1 + \text{SINR}_k). \quad (8)$$

The following proposition gives conditions for which the transmit power constraints are binding, i.e., transmitting at full power maximizes spectral efficiency.

Proposition 1. Let $c_{i,k} \triangleq d_{i,k}^{-\alpha} w_{i,k}$ denote the product of the antenna gains and the path-loss for link $i \rightarrow k$. Then setting $p_k = \text{psd}_{\max}$ for every k maximizes R in (8) if the following symmetry conditions hold:

- Every ground terminal k sees the same number of interfering satellites $|\mathcal{I}_k|$;
- $c_{i,i} = c_{k,k}$ for all i and k ;
- For every pair of terminals k and j , $c_k = [c_{i,k}]_{i \in \mathcal{I}_k}$ and $c_j = [c_{i,j}]_{i \in \mathcal{I}_j}$ contain the same elements.

The proof is in Appendix A.

C. Planar Approximation

For the following analysis we consider the approximation in which the surface of the earth is flat. The ground terminals and satellites then reside in parallel planes separated by h . That is, the satellite k has coordinates $(s_{k,1}, s_{k,2}, r_e + h)$, and terminal k has coordinates $(g_{k,1}, g_{k,2}, r_e)$. We also assume that the satellites and ground terminals extend to the infinite horizon

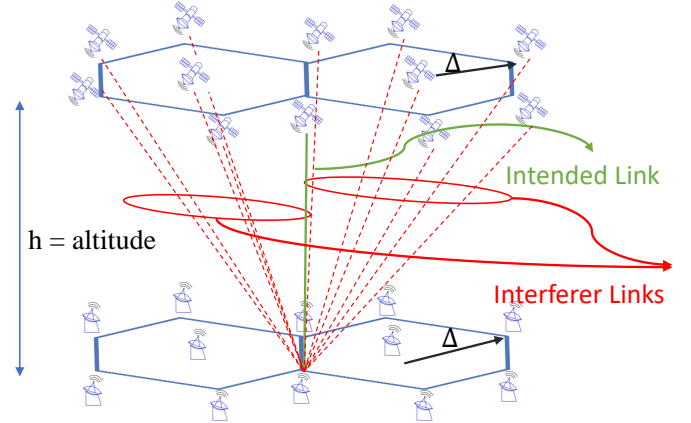


Fig. 3. Regular configuration of satellites and ground terminals in the planar model. The serving satellite is directly above the associated ground terminal.

(N is infinite), so that their density becomes the parameter of interest.

This approximation is pessimistic in that it includes interference from satellites that would be over the horizon in the spherical model. However, for scenarios where interference is dominated by neighboring satellites within a local region, the approximation will be accurate – for example, if the satellite network is dense or the beamwidths of the satellites and the ground users are narrow enough. We demonstrate numerically in Sec. VII-B that the flat-ground approximation is quite accurate when $r_e > 10h$.

D. Regular Configuration

Referring to Fig. 3, *regular placement* applied to the planar approximation means that the satellites and ground users are deployed across hexagonal lattices. To formally define this, we will index the satellite and ground stations by an ordered pair (i, j) with $i = j \pmod{2}$.

Definition 1. Let Δ denote the inter-satellite spacing, i.e., the distance between the adjacent satellites. We say the satellites are regularly placed if their locations are

$$s_{i,j}^{\text{reg}} \triangleq \left(i \frac{\Delta}{2}, j \frac{\Delta\sqrt{3}}{2}, r_e + h \right), \quad i = j \pmod{2}. \quad (9)$$

and the ground users are regularly placed if their locations are

$$g_{i,j}^{\text{reg}} \triangleq \left(i \frac{\Delta}{2}, j \frac{\Delta\sqrt{3}}{2}, r_e \right), \quad i = j \pmod{2}. \quad (10)$$

A *regular configuration* consists of regular placements of both satellites and ground terminals where satellite $s_{i,j}^{\text{reg}}$ serves ground terminal $g_{i,j}^{\text{reg}}$ and their antennas point directly to each other. Since the channel gains under this configuration satisfy the conditions in Proposition 1, the sum rate is maximized when all satellites transmit continuously at full power.

The regular configuration minimizes the lengths of all direct links, and so maximizes each received SNR, and maximizes the minimum distance between any pair of satellites. This

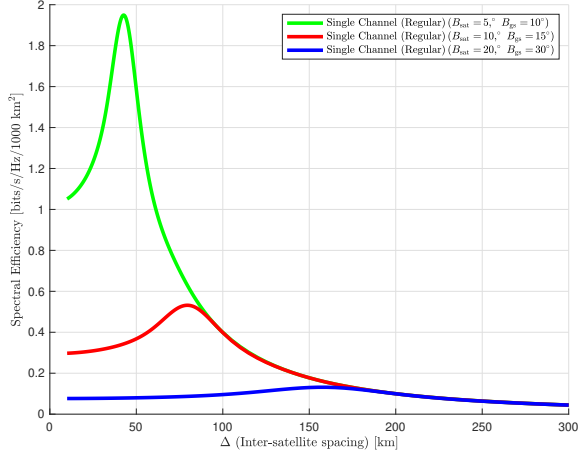


Fig. 4. Spectral efficiency versus inter-satellite spacing Δ for the regular configuration and the single channel model. The altitude $h = 550$ km, the serving link SNR is 10 dB, and beam patterns are given in Sec VII.

upper bounds the maximum interference between any pair of links.

Fig. 4 shows the spectral efficiency objective versus inter-satellite spacing for the single channel model with a regular configuration for three different sets of satellite and ground terminal first-null beamwidths B_{sat} and B_{gs} , respectively. We see that there is a unique peak corresponding to the optimal density that balances the increase in sum rate due to increasing number of satellites with the degradation due to interference. As the antenna patterns (beamwidths) widen, we observe that the optimal inter-satellite spacing increases.

IV. SPECTRAL EFFICIENCY FOR THE REGULAR CONFIGURATION

In this section, we assume the single-channel model with regularly placed satellites and characterize the positions of the ground terminals that maximize spectral efficiency. We then evaluate the spectral efficiency of the regular configuration (both single- and multi-channel).

A. Optimal Placement of Ground Terminals

We assume the satellites transmit with full power (i.e., psd_{max}), and point directly downward. We also assume that the ground terminals point directly upward. Thus the axes of all antenna patterns are perpendicular to the ground. Under these assumptions, we show that placing the terminals directly below the satellites maximizes the spectral efficiency.

Let $\mathbf{g} = (x, y, r_e)$ denote the position of a particular ground user. For any satellite corresponding to the indices (i, j) with $i = j \pmod{2}$, let $D_{i,j}(x, y) = \|\mathbf{s}_{i,j}^{\text{reg}} - \mathbf{g}\|$. The off-axis angle between the look direction of the satellite located at $\mathbf{s}_{i,j}^{\text{reg}}$ and the direction from the same satellite to the ground user located at \mathbf{g} can be expressed as

$$\theta_{i,j}(x, y) = \cos^{-1} \left(\frac{h}{D_{i,j}(x, y)} \right). \quad (11)$$

Note that the off-axis angle between the look direction of the ground user located at \mathbf{g} and the direction from the same

ground user to the satellite located at $\mathbf{s}_{i,j}$ is also equal to $\theta_{i,j}(x, y)$. Also let $W_{i,j}(x, y) \triangleq w_s(\theta_{i,j}(x, y))w_g(\theta_{i,j}(x, y))$ denote the combined attenuation from the satellite and ground user beam patterns.

Without loss of generality, assume the terminal at \mathbf{g} is served by the satellite located at $(0, 0, r_e + h)$. The SINR at the ground user can be expressed as

$$\text{SINR}(x, y) = \frac{\text{SNR}(x, y)}{\text{INR}(x, y) + 1}, \quad (12)$$

where

$$\text{SNR}(x, y) = \frac{\text{psd}_{\text{max}}}{\sigma^2} D_{0,0}^{-\alpha}(x, y) W_{0,0}(x, y), \quad (13)$$

$$\text{INR}(x, y) = \frac{\text{psd}_{\text{max}}}{\sigma^2} \sum_{(i,j) \in \mathcal{I}} D_{i,j}^{-\alpha}(x, y) W_{i,j}(x, y), \quad (14)$$

where $\mathcal{I} \triangleq \{(i, j) \mid i, j \in \mathbb{Z} \text{ and } i = j \pmod{2}\} \setminus \{(0, 0)\}$.

Proposition 2. *SINR(x, y) is maximized at $(x, y) = (0, 0)$ if the following conditions hold:*

- 1) *The antenna gain product $w_s(\theta)w_g(\theta)$ is a monotone decreasing function of $\theta \in [0, \pi]$,*
- 2) *$W_{i,j}(x, y)/W_{0,0}(x, y)$ is convex in x and y for $-\Delta/2 \leq x \leq \Delta/2$, $-\Delta\sqrt{3}/2 \leq y \leq \Delta\sqrt{3}/2$ and any $i = j \pmod{2}$.*

The proof is in Appendix B.

When the combined beam attenuation $W_{i,j}(x, y)$ satisfies the conditions in Proposition 2, the ground terminal associated with the satellite located at $(0, 0, h)$ must be located at $(0, 0, 0)$ to optimize the SINR. Likewise, the other ground terminals must be located directly below their associated satellites.

Antenna patterns typically exhibit non-monotonic behavior due to the presence of multiple nulls, so that Proposition 2 is not universally applicable. However, monotonic beam patterns that are upper or lower bounds on the actual beamforming patterns can be considered, which provide bounds on the received interference, and hence bound spectral efficiency. In particular, an upper bound on spectral efficiency can be obtained by ignoring the sidelobes. We verify numerically that the second condition in Proposition 2 holds for the beam patterns considered in Sec. VII.

B. Spectral Efficiency

We now evaluate the spectral efficiency objective as a function of psd_{max} and inter-satellite spacing Δ . Under the regular configuration, the SINRs for all ground users are identical. Consider the ground user located at $(0, 0, r_e)$. The off-axis angle between the look direction of satellite (i, j) and the direction from the satellite to the ground user located at $(0, 0, r_e)$ is

$$\theta_{i,j}^{\text{reg}}(\Delta) = \cos^{-1} (h / \|\mathbf{s}_{i,j}^{\text{reg}}\|). \quad (15)$$

The corresponding spectral efficiency is then

$$R^{\text{reg}}(\text{psd}_{\text{max}}, \Delta) = \frac{2}{\Delta^2 \sqrt{3}} \log_2 \left(1 + \frac{\gamma(\text{psd}_{\text{max}})}{\eta(\text{psd}_{\text{max}}, \Delta) + 1} \right) \quad (16)$$

where

$$\gamma(p) \triangleq \frac{p}{\sigma^2} h^{-\alpha}, \quad (17)$$

$$\eta(p, \Delta) \triangleq \frac{p}{\sigma^2} \sum_{(i,j) \in \mathcal{I}} \|s_{i,j}^{\text{reg}}\|^{-\alpha} w_s(\theta_{i,j}^{\text{reg}}(\Delta)) w_g(\theta_{i,j}^{\text{reg}}(\Delta)). \quad (18)$$

Although it is challenging to determine the optimal inter-satellite spacing Δ from (16) analytically, this single variable can be numerically optimized.

The following proposition characterizes the spectral efficiency of the regular configuration in the high-density regime.

Proposition 3. *As $\Delta \rightarrow 0$, $R^{\text{reg}}(\text{psd}_{\max}, \Delta)$ converges to a finite positive constant that depends on $\text{psd}_{\max}, \sigma^2, h, \alpha$ and the satellite and ground terminal beamwidths.*

The proof is in Appendix C.

Proposition 3 emphasizes the fact that the spectral efficiency does not increase without bound in the high density regime. In particular, Fig. 4 shows that the spectral efficiency converges to a constant below the finite maximum as $\Delta \rightarrow 0$. The spectral efficiency given by (16) applies for constant PSD constraints, independent of bandwidth.

As discussed in Sec. II-D, an upper bound on the achievable spectral efficiency of the wideband (multi-channel) satellite network is obtained by dividing the spectrum into narrow subbands and applying the optimal strategy per subband. Hence the spectral efficiency is upper bounded by

$$R \leq \frac{1}{B} \int_{\mathcal{B}} R^{\text{reg}}(\text{PSD}_{\max}(f), \hat{\Delta}(f)) df, \quad (19)$$

where

$$\hat{\Delta}(f) \triangleq \arg \max_{\Delta} R^{\text{reg}}(\text{PSD}_{\max}(f), \Delta). \quad (20)$$

V. SUBBAND ALLOCATION

When links are physically close and cause severe interference to each other, assigning them orthogonal subbands can be beneficial. The focus of this section is on allocating subbands across all links in order to maximize the overall spectral efficiency. Without loss of generality, we assume the positions and associations of satellites and ground users ($F(\cdot)$) are arbitrary, given, and remain fixed. Here, we also assume that each satellite uses a single spot beam to serve ground stations so that we drop the spot beam index from the notation.

A. Subband Allocation Problem

We will assume that all satellites transmit with a constant PSD so that for satellite i ,

$$P_i(f) = \begin{cases} \min\{\text{PSD}_{\max}(f), q_i\}, & \text{if } f \in \mathcal{B}_j, j \in S_i, \\ 0, & \text{otherwise,} \end{cases} \quad (21)$$

where q_i is chosen to satisfy the total power constraint

$$\sum_{j \in S_i} \int_{\mathcal{B}_j} P_i(f) df = \min \left\{ P_{\max}, \sum_{j \in S_i} \int_{\mathcal{B}_j} \text{PSD}_{\max}(f) df \right\}. \quad (22)$$

In other words, $P_i(f)$ may vary with the choice of $\{S_i\}_i$. The frequency-dependent SINR at ground terminal k is

$$\text{SINR}_k(f) = \frac{P_{F(k)}(f) \Omega_{F(k),k}(f)}{\sum_{i \neq F(k)} P_i(f) \Omega_{i,k}(f) + N_0}, \quad (23)$$

where $\Omega_{i,k}(f)$ is given by (3) so that the subband allocation problem can be formulated as

$$\begin{aligned} & \underset{\{S_i\}}{\text{maximize}} && \sum_k \sum_{j \in S_{F(k)}} \int_{\mathcal{B}_j} \log_2(1 + \text{SINR}_k(f)) df \\ & \text{subject to} && S_i \subseteq \{1, \dots, M\} \text{ for each } i. \end{aligned} \quad (24a)$$

$$(24b)$$

B. Hexagonal Frequency Reuse

The preceding subband allocation problem is combinatorial and difficult in the sense that there is unlikely to be a solution approach that scales with acceptable computational complexity for arbitrarily placed ground terminals. To proceed, we simplify the problem by superimposing a hexagonal structure on the ground terminals, as for a terrestrial cellular network. This enables a relatively straightforward subband assignment across ground terminals. Instead of solving (24), we determine $\{G_k\}_k$ for all ground stations. Then, satellites use the union of all frequencies corresponding to its associated ground stations. In other words, $S_i = \cup_{\{k:F(k)=i\}} G_k$ for any i .

We divide the frequency band \mathcal{B} into M disjoint subbands with equal bandwidths B/M .³ We then assign these subbands across hexagonal cells (one per hexagon) as in a cellular network where $M = m^2 + mn + n^2$ for non-negative integers m and n , and frequency reuse factor $1/M$. Letting L denote the channel reuse distance, the hexagons have sides of length $L/\sqrt{3M}$.

A ground terminal's Voronoi region is the set of all points in the plane closer to that terminal station than to any other terminal. If a terminal's Voronoi region contains the center of a hexagon, then that hexagon's subband is allocated to the terminal.

Fig. 5 shows an example of the hexagonal frequency reuse pattern superimposed on the Voronoi regions of the ground terminals for $M = 4$. The hexagon centers are represented by the digits 1–4. For example, the Voronoi region that includes the origin contains centers of two hexagons and should be allocated subbands $\{1, 3\}$; the adjacent Voronoi region to the upper left is allocated subband $\{1\}$. In the model presented here, a Voronoi region that does not contain a hexagonal center is not served. We defer numerical evaluation of the frequency reuse and subband allocation scheme to Sec. VII.

VI. SHUFFLING ASSOCIATIONS CAN INCREASE SPECTRAL EFFICIENCY

So far, we have associated satellites with ground terminals by minimizing a distance metric. (See also [13], [14], [20].) We have also proposed the regular configuration as a candidate for achieving the maximum spectral efficiency. In this section, we show that changing link directions and associations, which increases the previous distance metric, can reduce interference, and thereby increase spectral efficiency. In this section, a single channel model is assumed, i.e., satellites and ground stations use the same single narrow band.

Consider the example in Fig. 6 showing two different associations of a set of satellites with a set of ground terminals. We say two links strongly interfere if both the two satellites and the two ground terminals are neighbors. In that case,

³Note, this may require redefining the subbands so that they all have equal bandwidths.

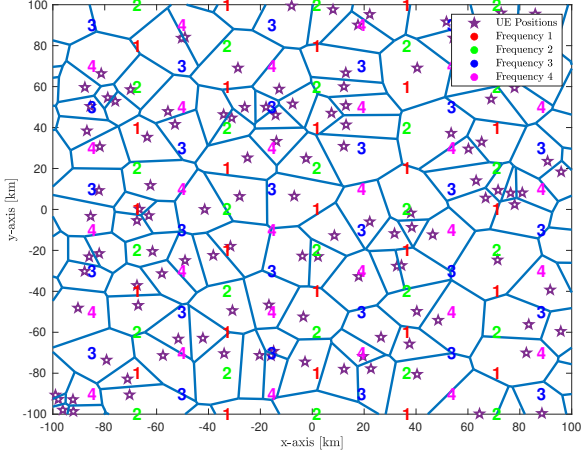


Fig. 5. Voronoi regions of randomly placed ground terminals on a plane along with the centers of the hexagonal frequency cells with $M = 4$ subbands.

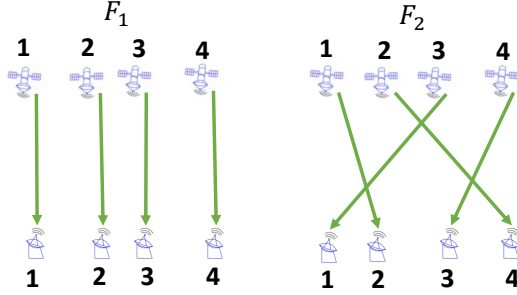


Fig. 6. Different associations between a set of satellites and ground terminals. The left minimizes a distance metric whereas the right has lower interference at each terminal.

each link is said to be a strong interferer for the other. With the association depicted on the left in Fig. 6, every link has one or two strong interferers. In contrast, with the association depicted on the right, no links strongly interfere. Furthermore, if the inter-satellite spacing is small, the direct link gains do not degrade significantly by switching from the left to the right association.

We propose the following simple heuristic method to determine an association that avoids strong interference. If two satellites are close to each other, within a distance Δ_s , they are assigned to ground terminals separated by minimum distance Δ_g , where Δ_s and Δ_g are design parameters. For any i, k , we desire an association $F(\cdot)$ to satisfy

$$\|\mathbf{s}_{F(i)} - \mathbf{s}_{F(k)}\| \leq \Delta_s \implies \|\mathbf{g}_i - \mathbf{g}_k\| > \Delta_g. \quad (25)$$

Next, we provide an algorithm to improve the spectral efficiency of the regularly placed satellites and ground users.

A. Shuffling Algorithm

We start with the regular configuration along a single dimension as shown in Fig. 6 where the number of satellites (or ground stations) is 2^j for natural number j . Given the

satellite index $k \in \{1, \dots, 2^j\}$, we define the mapping to ground station index as

$$f^{(j)}(k) = \begin{cases} \frac{k+2^j+1}{2}, & \text{if } k \text{ is odd,} \\ \frac{k}{2}, & \text{if } k \text{ is even.} \end{cases} \quad (26)$$

According to (26), two nearest-neighbor satellites are mapped to two ground stations that are separated by at least 2^{j-1} . We extend this mapping to $k > 2^j$, i.e., to a satellite in an adjacent block of 2^j satellites, using the periodic mapping

$$f^{(j)}(k) = 2^j \left\lfloor \frac{k-1}{2^j} \right\rfloor + f^{(j)}\left(k - 2^j \left\lfloor \frac{k-1}{2^j} \right\rfloor\right). \quad (27)$$

For the regular configuration of satellites/ground stations in a plane, let $F_x(\cdot), F_y(\cdot) : \mathbb{Z} \rightarrow \mathbb{Z}$ denote associations over the x and y axes, respectively. Both $F_x(\cdot)$ and $F_y(\cdot)$ are determined by applying the same procedure where we shuffle the mapping from satellites to ground stations along each dimension. We can then iterate the shuffling algorithm, that is, repeatedly apply the mapping (27) to the current set of associations. Parameters for this procedure are then the shuffling block sizes $D_x = 2^{n_x}, D_y = 2^{n_y}$ for integers $n_x, n_y \geq 1$, and the numbers of shuffling rounds ℓ_x, ℓ_y for $F_x(\cdot)$ and $F_y(\cdot)$, respectively, where $\ell_x \leq n_x - 1$ and $\ell_y \leq n_y - 1$.

Specifically, when there is a single round of shuffling, $\ell_x = 1$ and $F_x(m) = f^{(n_x)}(m)$. In general, for arbitrary ℓ_x and n_x , the shuffling strategy is given by

$$F_x(m) = f^{(n_x - \ell_x + 1)}\left(f^{(n_x - \ell_x + 2)}\left(\dots\left(f^{(n_x)}(m)\right)\dots\right)\right). \quad (28)$$

Figs. 7(a) and 7(b) illustrate the results of one and two rounds of shuffling in one dimension ($\ell = 1$ and $\ell = 2$) with $D = 8$. Iterating the shuffling (i.e., adding a shuffling round, going from Fig. 7(a) to Fig. 7(b)) increases the minimum distance from the serving satellites to neighboring ground users. However, it also generally increases the distance between the serving satellite and its ground user. As the density becomes large so that the inter-satellite spacing Δ becomes small, the incremental increase in the direct path attenuation due to an additional shuffling iteration may be offset by the decrease in interference thereby increasing spectral efficiency.

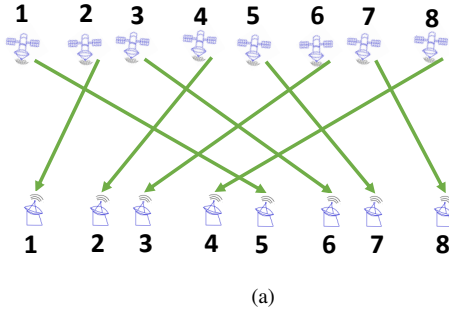
To extend the shuffling procedure to two dimensions, recall that the regular satellite locations $\mathbf{s}_{i,j}^{\text{reg}}$ and ground user locations $\mathbf{g}_{i,j}^{\text{reg}}$ are given by (9) and (10), respectively. We shuffle the association rules over the x and y axes independently. Letting $F^{\text{shuffle}}(i, j)$ denote the shuffled (x, y) indices of the ground station $\mathbf{g}_{i,j}^{\text{reg}}$ associated with $\mathbf{s}_{i,j}^{\text{reg}}$, we can write

$$F^{\text{shuffle}}(i, j) = \left(2F_x\left(\frac{i-q}{2}\right) + r, F_y(j)\right), \quad (29)$$

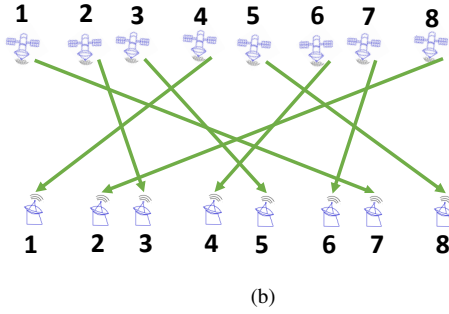
where $q \in \{0, 1\}$ is the remainder when i is divided by 2 and $r \in \{0, 1\}$ is the remainder when $F_y(j)$ is divided by 2.

B. Spectral Efficiency Upper Bound: Regular Configuration

We present an upper bound on the spectral efficiency for regularly placed satellites and ground terminals using a single-channel. As defined in Sec. II-C, the look directions of the satellites and terminals are upper bounded by γ_s and γ_g , respectively. For any particular terminal, all interfering satellites are located in the beam region of the terminal. Hence the distance from any interfering satellite to the terminal must be



(a)



(b)

Fig. 7. Shuffling strategies when $D = 8$ and $\ell = 1$ in (a) and $\ell = 2$ in (b).

smaller than $h\sqrt{1 + \tan^2(\gamma_g/2)}$. Furthermore, by assuming monotonic antenna patterns, the antenna gain between the terminal and any satellite in the beam region is lower bounded by $w_s(\gamma_s)w_g(\gamma_g)$, i.e., assuming they look away from each other at the maximum angle.

Therefore, the aggregate interference at any particular terminal is lower bounded by

$$I_{\min} \triangleq \text{psd}_{\max} (h^2 + h^2 \tan^2(\gamma_g/2))^{-\frac{\alpha}{2}} w_s(\gamma_s)w_g(\gamma_g). \quad (30)$$

The spectral efficiency is then upper bounded by

$$R^{\text{reg}}(\text{psd}_{\max}, \Delta) \leq \frac{2}{\Delta^2 \sqrt{3}} \log_2 \left(1 + \frac{\text{psd}_{\max} h^{-\alpha}}{X I_{\min} + N_0} \right), \quad (31)$$

where X is the number of interfering satellites in the beam region of the ground terminal, and can be computed by counting the number of pairs (i, j) with the same parity such that

$$i^2 + 3j^2 \leq \frac{4h^2 \tan^2(\gamma_g/2)}{\Delta^2}. \quad (32)$$

VII. NUMERICAL RESULTS

A. Antenna Patterns and System Parameters

We use the antenna pattern given in [22], [23] for both the satellites and the terminals. Given off-axis angle θ and first-null beamwidth B , the antenna pattern is expressed as

$$g(B, \theta) = \begin{cases} 1, & \text{if } \theta = 0^\circ \\ 4 \left| \frac{J_1(K \sin \theta)}{K \sin \theta} \right|^2, & \text{for } 0^\circ \leq |\theta| \leq 90^\circ, \end{cases} \quad (33)$$

where $J_1(\cdot)$ is the first order Bessel function of the first kind and K determines the beamwidth. That is, the corresponding beamwidth is⁴ $B = \sin^{-1}(3.8317/K)$.

Unless noted otherwise, we set beam regions $\gamma_s = \gamma_g = 90^\circ$, i.e., satellites and ground users can point to anywhere. Given satellite and ground terminal beamwidths B_{sat} and B_{gs} , the associated antenna patterns are

$$w_s(\theta) \triangleq g(B_{\text{sat}}, \theta), \quad w_g(\theta) \triangleq g(B_{\text{gs}}, \theta). \quad (34)$$

For the examples in this section we assume that $h = 550$ km, the path-loss exponent $\alpha = 2.5$ and $\text{PSD}_{\max}(f) = \text{psd}_{\max}$ for all $f \in \mathcal{B}$. In addition, we assume all path attenuations are frequency-nonselective.

B. Planar Approximation

Fig. 8 compares the spectral efficiency of the spherical model with the planar approximation described in Sec. III-C. Consider the terminal located at $(0, 0, r_e)$. Any satellite whose zenith angle is smaller than $\theta_f \triangleq \cos^{-1}(r_e/(r_e + h))$ lies in the field-of-view of the ground terminal. We generate N satellites in the field-of-view of the terminal according to the Binomial Point Process (BPP). From [24, Prop. 1], the location of a satellite can be written as $(r_e + h)[\sin \zeta \cos \varphi \quad \sin \zeta \sin \varphi \quad \cos \zeta]$, where $\varphi \sim \mathcal{U}[0, 2\pi]$ and the cumulative distribution function of ζ is given as

$$F_\zeta(\theta) = (1 - \cos \theta)/(1 - \cos \theta_f), \quad 0 \leq \theta \leq \theta_f. \quad (35)$$

Similarly, we generate $(N - 1)$ ground terminals according to the BPP on the Earth's surface in addition to the terminal at $(0, 0, r_e)$. Zenith angles of these terminals are assumed to be in $[0, \theta_f]$, and azimuth angles are uniformly distributed between 0 and 2π . Associations between the satellites and terminals are determined by minimizing the total distance metric (6). Look directions of the satellite-terminal pairs are aligned. For the planar approximation, we project satellite locations to the two-dimensional plane $\{(x, y, r_e + h) \mid x, y \in \mathbb{R}\}$. Specifically, the satellite location (x, y, z) is projected to $(x\rho, y\rho, z\rho)$, where $\rho = (r_e + h)/z$. Similarly, we project terminal locations to the two-dimensional plane $\{(x, y, r_e) \mid x, y \in \mathbb{R}\}$.

Fig. 8 compares averages of $\log_2(1 + \text{SINR})$ over satellite and terminal locations at the fixed terminal location $(0, 0, r_e)$ for both the BPP-spherical model and planar approximation. In this example, all satellites transmit at power P_{\max} and use the entire bandwidth. We consider three different sets of beamwidths $(B_{\text{sat}}, B_{\text{gs}})$, namely, $(10^\circ, 20^\circ)$, and $(30^\circ, 40^\circ)$. The serving link SNR is 8 dB. Fig. 8 indicates that the planar model is quite accurate for parameters of interest. Hence for computational ease, all subsequent plots are generated for the planar model.

C. Comparisons with Random Configuration

We present a series of plots illustrating the performance with satellites and ground terminals dropped uniformly and associated to minimize the distance metric (6). We also let their look directions be aligned.

Fig. 9 compares spectral efficiencies versus inter-satellite spacing corresponding to randomly and regularly-placed satellite networks for a single channel network. Results are again

⁴Both the half-power and full-null beamwidths are determined solely by the parameter K . The half-power beam-width is given by $\sin^{-1}(1.6216/K)$.

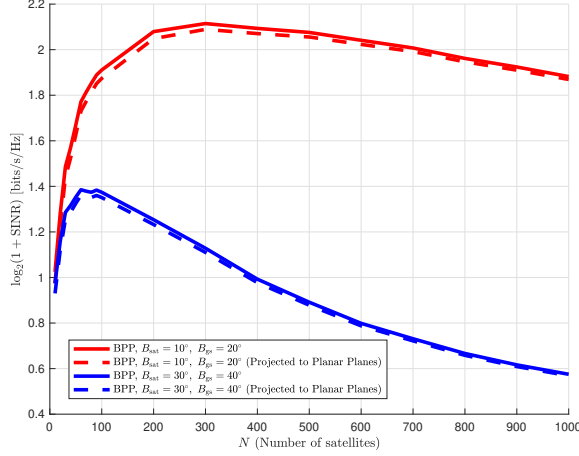


Fig. 8. The individual rate (bits/s/Hz) at the ground terminal located at $(0, 0, r_e)$ versus the number of satellites within the field-of-view (N) for the BPP model and planar approximation.

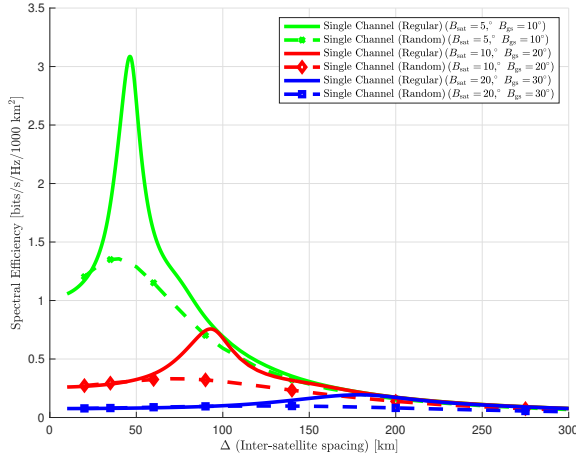


Fig. 9. Spectral efficiency versus inter-satellite spacing with randomly and regularly placed satellites and terminals with a single channel. Results are shown for three sets of beamwidths.

shown for three sets of beamwidths. For the random configuration, Δ denotes the expected inter-satellite spacing. The figure indicates the spectral efficiency achieved by the regular configuration upper bounds that of the random configuration with the minimum distance association between satellites and ground terminals. In addition, for very small values (or very large) of Δ , regular and random have similar spectral efficiencies.

Fig. 10 shows spectral efficiency versus inter-satellite spacing for multi-channel satellite networks. Each satellite can serve N_B different ground users, where $N_B \in \{10, 20\}$. In other words, the number of ground stations is equal to N_B times the number of satellites. Associations between satellites and terminals are again based on minimizing the distance metric (6). Locations of the satellites and the ground terminals are generated uniformly and subband allocation algorithm in Sec. V is used to assign subbands to links. Power is set so that $P_{\max} h^{-\alpha} / (B\sigma^2)$ is 8 dB and $\text{psd}_{\max} =$

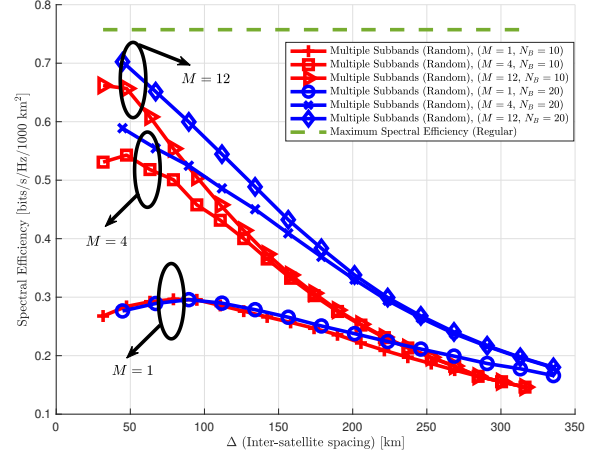


Fig. 10. Spectral efficiency versus inter-satellite spacing with random placements and multiple channels. Also shown is the upper bound for the regular configuration. Parameters are $\text{psd}_{\max} = 10P_{\max}/B$, $(B_{\text{sat}}, B_{\text{gs}}) = (10^\circ, 20^\circ)$, number of subbands $M = 1, 4, 12$ and each satellite serves $N_B = 10$ or $N_B = 20$ ground stations.

M	1	4	7	12	19
$\Delta = 50$ km	0.286	0.363	0.371	0.376	0.376
$\Delta = 200$ km	0.072	0.072	0.072	0.072	0.072

TABLE I
SPECTRAL EFFICIENCY [BITS/SEC/Hz/1000 km²] FOR DIFFERENT NUMBERS OF SUBBANDS (M) AND SPACINGS (Δ).

$10P_{\max}/B$. The satellite and the terminal beamwidths are $(B_{\text{sat}}, B_{\text{gs}}) = (10^\circ, 20^\circ)$.

Also, the maximum value of the spectral efficiency over all choices of Δ in a regular configuration (i.e., the peak value in Fig. 9) is plotted as a horizontal line for $(B_{\text{sat}}, B_{\text{gs}}) = (10^\circ, 20^\circ)$. Plots are shown for $M = 1, 4$, and 12 subbands. For each inter-satellite spacing Δ , the optimal co-channel distance for the hexagonal array is found numerically. Increasing the number of subchannels offers a substantial increase in spectral efficiency for small values of Δ (dense network), but that increase in spectral efficiency diminishes substantially when $\Delta \geq 330$ km. Fig. 10 also shows that there is an optimal spacing Δ^* , which maximizes spectral efficiency, so that interference limits performance for $\Delta < \Delta^*$. As the number of subchannels or N_B increases, Δ^* decreases, and the figure shows that with $M = 12$ subchannels, the performance approaches the maximum spectral efficiency for the regular configuration for small Δ .

Table I shows spectral efficiency as a function of the number of subbands for the randomly placed network. Possible values for the number of subbands, M , are in the form of $m^2 + mn + n^2$ as discussed in Sec. V-B. Here we assume that psd_{\max} is not a binding constraint. We consider the power-limited scenario $P_{\max} h^{-\alpha} / B\sigma^2 = 8$ dB with $(B_{\text{sat}}, B_{\text{gs}}) = (10^\circ, 20^\circ)$ and two different satellite spacings: $\Delta = 200$ km and $\Delta = 50$ km. The former is intended to correspond roughly to current satellite spacings, and the latter corresponds to a much denser network. The results show that the spectral efficiency does not change with respect to the number of subbands when $\Delta = 200$ km. When $\Delta = 50$ km, the

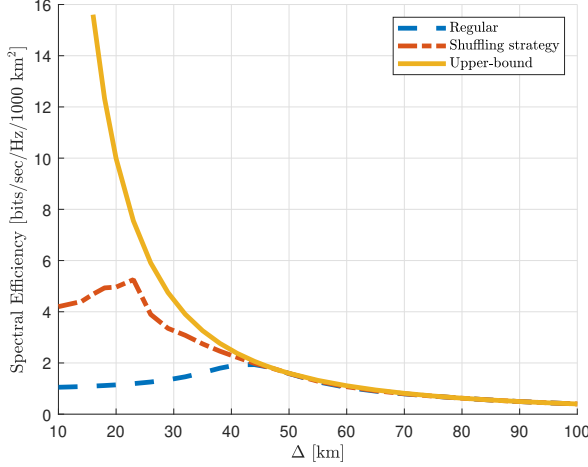


Fig. 11. Spectral efficiency versus the inter-satellite spacing for both minimum-distance and shuffled associations along with the upper bound in (31) for the regularly placed network, when $(B_{\text{sat}}, B_{\text{gs}}) = (5^\circ, 10^\circ)$, $\text{psd}_{\text{max}} h^{-\alpha}/\sigma^2 = 10$ dB, $\gamma_s = \gamma_g = 40^\circ$.

spectral efficiency increases with the number of subbands up to $M = 12$, and then remain basically constant, limited only by the SNR constraint rather than interference.⁵

D. Shuffling Strategy

The spectral efficiencies of the shuffling strategy and the distance based association for the regular configuration along with the upper bound given in (31) are plotted in Fig. 11. The direct link gain $\text{psd}_{\text{max}} h^{-\alpha}/\sigma^2$ is set to 10 dB. The satellite and the ground terminal beamwidths are chosen as $(B_{\text{sat}}, B_{\text{gs}}) = (5^\circ, 10^\circ)$. We set $\gamma_s = \gamma_g = 40^\circ$.

For the shuffling strategy, because of the beam region constraints, possible (D_x, D_y) pairs for $F_x(\cdot)$ and $F_y(\cdot)$ are chosen to satisfy $(D_x \Delta)^2 + (D_y \Delta \sqrt{3}/2)^2 \leq h^2 \tan(\gamma_g/2)^2$ for any given Δ . This inequality implies that associated satellites and ground terminals lie within the corresponding beam regions, hence we can assume their look-directions are perfectly aligned. For all (D_x, D_y) pairs satisfying the preceding inequality, we search over all possible values of (ℓ_x, ℓ_y) to obtain the highest possible spectral efficiency.

Fig. 11 shows that shuffling achieves a substantial increase in spectral efficiency for small Δ relative to distance-based association. As Δ increases, the performance improvement diminishes, falling to near zero for $\Delta \geq 42$ km.

In existing deployments, the inter-satellite spacing is larger than 100 km. At such densities, the upper bound in Fig. 11 is tight, and the spectral efficiency is well under 1 bits/s/Hz/1000 km². As a reference, at 0.1 bits/s/Hz/1000 km², the total throughput to Earth over 1 GHz band is under 52 Tbits/s. In contrast, the total capacity has been estimated to be 3 Tbits/s for constellations proposed by the leading operators using current technologies [1].⁶

E. Comparison with Fading

⁵In practice, the probability of an in-line interference event is also an important performance metric, so that additional bandwidth may be needed to ensure that this is sufficiently small.

⁶This calculation does not discount the throughput to uninhabited areas.

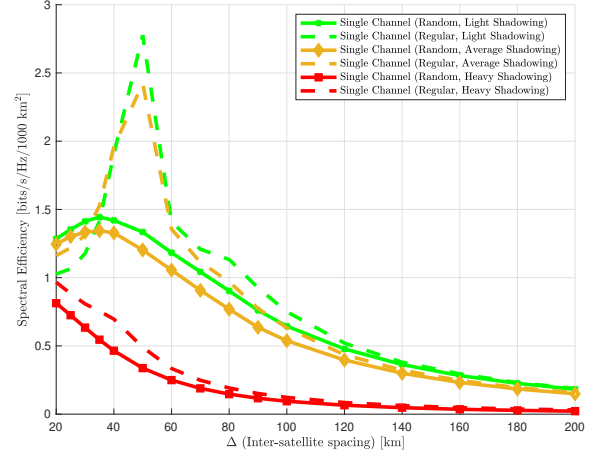


Fig. 12. Spectral efficiency versus inter-satellite spacing for random and regular configurations under light, average and heavy shadowing scenarios when $(B_{\text{sat}}, B_{\text{gs}}) = (5^\circ, 10^\circ)$, $\text{psd}_{\text{max}} h^{-\alpha}/\sigma^2 = 18$ dB.

Fig. 12 compares the spectral efficiencies of regular and random configurations with Shadowed Rician (SR) fading. Specifically, the link gain from satellite i to terminal j is given by $d_{j,i}^{-\alpha} w_{j,i} \xi_{j,i}$, where $d_{j,i}$ and $w_{j,i}$ are defined in Sec. III, and $\xi_{j,i}$ is the random satellite-to-terminal attenuation for link (i, j) . Let the attenuations $\xi_{j,i}$ be independent and identically distributed shadowed Rician random variables, where the average power of the non-line-of-sight component is equal to $2b$, the average power of the line-of-sight component is equal to ω , and the fading order is m [23], [25]. The values of b, m, ω for light, average, and heavy shadowing scenarios are available in [23]. We simulate a single-channel network where the associations are determined according to the distance criterion. The results show that with fading the regular configuration still upper bounds the random configuration, and that this bound appears to be significantly tighter when compared to the results without fading.

VIII. CONCLUSIONS

Given the trend towards denser satellite networks, improved resource allocation methods can offer significant gains in spectral efficiency. Our results indicate that the current density of satellites is well below the density at which interference is likely to become the dominant impairment that limits the overall sum rate. We have proposed the so-called regular configuration of satellites and ground users as a benchmark for obtaining meaningful bounds on the sum spectral efficiency. In the interference-limited regime, we have presented subchannel allocation and beam-pointing strategies that can lead to a substantial improvement in spectral efficiency.

Proving the sum-rate optimality of the regular configuration with minimum-distance associations remains an open problem. In general, determining the maximum spectral efficiency for a LEO network treating locations, associations, and frequency assignments as optimization variables is quite complicated. Moreover, in this work full coordination among the satellites is assumed whereas in practice there may be several service providers that compete to serve the customer base. Such scenarios without full coordination, including distributed, contention-based resource allocation, is left for future work.

APPENDIX A
PROOF OF PROPOSITION 1

First, we can re-write SINR_k in (7) as

$$\text{SINR}_k = \frac{p_k c_{k,k}}{\sum_{i \in \mathcal{I}_k} p_k c_{i,k} + \sigma^2}, \quad (36)$$

for any k . As $\log_2(1+x)$ is a concave function of x , by Jensen's inequality, we can write

$$\frac{1}{N} \sum_{k=1}^N \log_2(1 + \text{SINR}_k) \leq \log_2 \left(1 + \frac{1}{N} \sum_{k=1}^N \text{SINR}_k \right), \quad (37)$$

where the equality is satisfied only if SINR_k s are identical. Let u and v be defined as

$$u = \arg \max_k p_k \text{ and } v = \arg \min_k p_k. \quad (38)$$

The condition $\text{SINR}_u = \text{SINR}_v$ implies that

$$\frac{p_v c_{v,v}}{\sum_{i \in \mathcal{I}_v} p_i c_{i,v} + \sigma^2} = \frac{p_u c_{u,u}}{\sum_{i \in \mathcal{I}_u} p_i c_{i,u} + \sigma^2}. \quad (39)$$

As $c_{v,v} = c_{u,u}$, (39) reduces to

$$\sum_{i \in \mathcal{I}_v} \frac{p_i}{p_v} c_{i,v} + \frac{\sigma^2}{p_v} = \sum_{i \in \mathcal{I}_u} \frac{p_i}{p_u} c_{i,u} + \frac{\sigma^2}{p_u}. \quad (40)$$

As $\{c_{i,v}\}_{i \in \mathcal{I}_v}$ is a permutation of $\{c_{i,u}\}_{i \in \mathcal{I}_u}$, there exists a bijection $\tilde{\sigma}(\cdot)$ from \mathcal{I}_v to \mathcal{I}_u such that

$$c_{i,v} = c_{\tilde{\sigma}(i),u} \quad (41)$$

for any $i \in \mathcal{I}_v$. Hence, (40) can be re-written as

$$\sum_{i \in \mathcal{I}_v} \left(\frac{p_i}{p_v} - \frac{p_{\tilde{\sigma}(i)}}{p_u} \right) c_{i,v} = \frac{\sigma^2}{p_u} - \frac{\sigma^2}{p_v} \quad (42)$$

Since $p_{\tilde{\sigma}(i)} \leq p_u$ and $p_v \leq p_i$ for any $i \in \mathcal{I}_v$, we can conclude that

$$\sum_{i \in \mathcal{I}_v} \left(\frac{p_i}{p_v} - \frac{p_{\tilde{\sigma}(i)}}{p_u} \right) c_{i,v} \geq 0. \quad (43)$$

Moreover, by (38),

$$\frac{\sigma^2}{p_u} - \frac{\sigma^2}{p_v} \leq 0. \quad (44)$$

By combining (42), (43) and (44), we can conclude that all SINR_k s are equal only if $p_v = p_u$, equivalently, all p_i s are equal to each other.

Let $p_k = p$ for any k . Then, if we take the derivative of SINR_k with respect to p , we obtain

$$\frac{\partial \text{SINR}_k}{\partial p} = \frac{c_{k,k} \sigma^2}{(\sum_{i \in \mathcal{I}_k} p c_{i,k} + \sigma^2)^2} \geq 0. \quad (45)$$

Therefore, to maximize $\sum_{k=1}^N \log_2(1 + \text{SINR}_k)$, we must have $p_k = \text{psd}_{\max}$ for any k . \square

APPENDIX B
PROOF OF PROPOSITION 2

Lemma 1. Assuming $w_s(\theta)w_g(\theta)$ is a monotone-decreasing function of $\theta \in [0, \pi]$, $(\hat{x}, \hat{y}) = \arg \max_{x,y} \text{SINR}(x,y)$ implies that $-\Delta/2 \leq \hat{x} \leq \Delta/2$ and $-\Delta\sqrt{3}/2 \leq \hat{y} \leq \Delta\sqrt{3}/2$.

Proof. Take any $x, y \in \mathbb{R}$ with $x \geq \Delta/2$. Note that

$$\begin{aligned} \frac{\text{SINR}(x - \Delta, y)}{\text{SINR}(x, y)} &= \frac{D_{0,0}^{-\alpha}(x - \Delta, y) W_{0,0}(x - \Delta, y)}{D_{0,0}^{-\alpha}(x, y) W_{0,0}(x, y)} \\ &= \frac{D_{2,0}^{-\alpha}(x, y) W_{2,0}(x, y)}{D_{0,0}^{-\alpha}(x, y) W_{0,0}(x, y)}, \end{aligned} \quad (46)$$

and

$$\begin{aligned} \text{INR}(x, y) - \text{INR}(x - \Delta, y) &= \\ \frac{\text{psd}_{\max}}{\sigma^2} (D_{2,0}^{-\alpha}(x, y) W_{2,0}(x, y) - D_{0,0}^{-\alpha}(x, y) W_{0,0}(x, y)). \end{aligned} \quad (47)$$

It is possible to write that,

$$\begin{aligned} D_{2,0}(x, y) &= \sqrt{(x - \Delta)^2 + y^2 + h^2} \\ &\leq \sqrt{x^2 + y^2 + h^2} = D_{0,0}(x, y), \end{aligned} \quad (48)$$

and

$$\begin{aligned} \theta_{2,0}(x, y) &= \cos^{-1} \left(h / \sqrt{(x - \Delta)^2 + y^2 + h^2} \right) \\ &\leq \cos^{-1} \left(h / \sqrt{x^2 + y^2 + h^2} \right) = \theta_{0,0}(x, y). \end{aligned} \quad (49)$$

We can argue that

$$\theta_{0,0}(x, y) \leq \theta_{2,0}(x, y) \implies W_{0,0}(x, y) \leq W_{2,0}(x, y), \quad (50)$$

as $w_s(\cdot)w_g(\cdot)$ is non-increasing in $[0, \pi]$.

As a consequence of (46)-(50), we can conclude that $\text{SINR}(x - \Delta, y) \geq \text{SINR}(x, y)$. Similarly, one can show that for any $x \leq -\Delta/2$, $\text{SINR}(x + \Delta, y) \geq \text{SINR}(x, y)$. In addition, we can prove that for any $y \geq \Delta\sqrt{3}/2$, we have $\text{SINR}(x, y - \Delta\sqrt{3}/2) \geq \text{SINR}(x, y)$ and for any $y \leq -\Delta\sqrt{3}/2$, we have $\text{SINR}(x, y + \Delta\sqrt{3}/2) \geq \text{SINR}(x, y)$. Thus, we conclude that the we can focus on the intervals $-\Delta/2 \leq x \leq \Delta/2$ and $-\Delta\sqrt{3}/2 \leq y \leq \Delta\sqrt{3}/2$. \square

Lemma 2. For any $i = j \pmod{2}$ and $(i, j) \neq (0, 0)$, define

$$\rho_{i,j}(x, y) \triangleq \left(\frac{D_{0,0}(x, y)}{D_{i,j}(x, y)} \right)^2, \quad (51)$$

Then, $\rho_{i,j}(x, y)$ is convex in both x and y for $-\Delta/2 \leq x \leq \Delta/2$ and $-\Delta\sqrt{3}/2 \leq y \leq \Delta\sqrt{3}/2$.

Proof. We will prove the convexity of $\rho_{i,j}(x, y)$ when i and j are even. The other case, i.e., $i = j = 1 \pmod{2}$ can be proven similarly.

Let $a = i/2$, $b = j/2$, $\ell = y^2 + h^2$, and $m = (y - \Delta\sqrt{3}b)^2 + h^2$. It should be noted that

$$\ell - m = (2y - \Delta\sqrt{3}b)\Delta\sqrt{3}b \leq 0, \quad (52)$$

for any $b \in \mathbb{Z}$.

After some algebraic manipulations, it is easily verified that in order to show the convexity of $\rho_{i,j}(x, y)$ in x , the following inequality must hold

$$\begin{aligned} (x - \Delta a)^2 (\Delta^2 a^2 + 2\Delta a x + 3\ell) \\ + m(m - \ell + 2\Delta^2 a^2 - 3x^2) \geq 0 \end{aligned} \quad (53)$$

1) Case I: ($a = 0$) After rearranging (53), we must prove the following inequality

$$(m - \ell)(m - 3x^2) \geq 0. \quad (54)$$

Then, (54) reduces to $m \geq 3x^2$ due to (52). Since $(i, j) \neq (0, 0)$, b cannot be equal to 0. In other words, $|b| \geq 1$. Note that

$$m = (y - \Delta\sqrt{3}b)^2 + h^2 > (y - \Delta\sqrt{3}b)^2 \geq \frac{3\Delta^2}{4} \geq 3x^2 \quad (55)$$

as we desired to prove.

2) Case II: ($a \neq 0$)

First, note that

$$\Delta^2 a^2 + 2\Delta ax \geq 0, \quad (56)$$

for any $a \in \mathbb{Z}$.

Secondly, as $x^2 \leq \Delta^2/4$

$$2\Delta^2 a^2 - 3x^2 \geq 0, \quad (57)$$

for any $a \neq 0$. Therefore, (54) is true by combining (56) and (57).

Thus, we prove the convexity of $\rho_{i,j}(x, y)$ in x when $i = j = 0 \pmod{2}$. The proof of convexity in y can be done similarly. \square

As a consequence of Lemma 1, we can restrict our attention to the intervals $-\Delta/2 \leq x \leq \Delta/2$ and $-\Delta\sqrt{3}/2 \leq y \leq \Delta\sqrt{3}/2$. We also assume $x, y \geq 0$. The other three cases regarding the signs of x and y can be considered similarly.

We can write

$$\begin{aligned} \frac{1}{\text{SNR}(x, y)} &= \sum_{(i,j) \in \mathcal{I}} \frac{D_{i,j}^{-\alpha}(x, y) W_{i,j}(x, y)}{D_{0,0}^{-\alpha}(x, y) W_{0,0}(x, y)} + \frac{1}{\text{SNR}(x, y)} \\ &= \sum_{(i,j) \in \mathcal{I}} \frac{W_{i,j}(x, y)}{W_{0,0}(x, y)} \rho_{i,j}^{\alpha/2}(x, y) + \frac{1}{\text{SNR}(x, y)}. \end{aligned} \quad (58)$$

Due to Lemma 2, $\rho_{i,j}(x, y)$ is convex in x and y . Hence, for $\alpha > 2$, we can easily note that $\rho_{i,j}^{\alpha/2}(x, y)$ is convex in x and y as well. Then we can argue for any $i, j \geq 1$ that

$$\rho_{2i,2j}^{\alpha/2}(x, y) + \rho_{2i,2j}^{\alpha/2}(-x, y) \geq 2\rho_{2i,2j}^{\alpha/2}(0, y). \quad (59)$$

In addition, from the second condition in Proposition 2, we can write

$$\frac{W_{2i,2j}(x, y)}{W_{0,0}(x, y)} + \frac{W_{2i,2j}(-x, y)}{W_{0,0}(x, y)} \geq 2 \frac{W_{2i,2j}(0, y)}{W_{0,0}(0, y)}, \quad (60)$$

It is also clear that

$$\frac{W_{2i,2j}(x, y)}{W_{0,0}(x, y)} \geq \frac{W_{2i,2j}(-x, y)}{W_{0,0}(x, y)} = \frac{W_{-2i,2j}(x, y)}{W_{0,0}(x, y)}, \quad (61)$$

$$\rho_{2i,2j}(x, y) \geq \rho_{2i,2j}(-x, y) = \rho_{-2i,2j}(x, y). \quad (62)$$

Then, by using the rearrangement inequality, we reach that

$$\frac{W_{2i,2j}(x, y)}{W_{0,0}(x, y)} \rho_{2i,2j}^{\alpha/2}(x, y) + \frac{W_{-2i,2j}(x, y)}{W_{0,0}(x, y)} \rho_{-2i,2j}^{\alpha/2}(x, y) \quad (63)$$

$$\geq 2 \frac{W_{2i,2j}(0, y)}{W_{0,0}(0, y)} \rho_{2i,2j}^{\alpha/2}(0, y). \quad (64)$$

Similarly, we have

$$\frac{W_{2i,-2j}(x, y)}{W_{0,0}(x, y)} \rho_{2i,-2j}^{\alpha/2}(x, y) + \frac{W_{-2i,-2j}(x, y)}{W_{0,0}(x, y)} \rho_{-2i,-2j}^{\alpha/2}(x, y) \quad (65)$$

$$\geq 2 \frac{W_{2i,-2j}(0, y)}{W_{0,0}(0, y)} \rho_{2i,-2j}^{\alpha/2}(0, y) = 2 \frac{W_{2i,2j}(0, -y)}{W_{0,0}(0, -y)} \rho_{2i,2j}^{\alpha/2}(0, -y). \quad (66)$$

By using convexity in y and doing the same steps above, we can claim that

$$(0, 0) = \arg \min_{(x,y) \in \mathbb{R}^2} \sum_{(i,j) \neq (0,0)} \frac{D_{2i,2j}^{-\alpha}(x, y) W_{2i,2j}(x, y)}{D_{0,0}^{-\alpha}(x, y) W_{0,0}(x, y)}. \quad (67)$$

Similarly, we can prove that

$$(0, 0) = \arg \min_{(x,y) \in \mathbb{R}^2} \sum_{i,j} \frac{W_{2i+1,2j+1}(x, y)}{W_{0,0}(x, y)} \rho_{2i+1,2j+1}(x, y). \quad (68)$$

As $(0, 0)$ is the maximizer of $\text{SNR}(x, y)$, we reach the desired conclusion. \square

APPENDIX C PROOF OF PROPOSITION 3

Let us define $D_{i,j}^{\text{reg}}(\Delta)$ as the distance of the satellite located at $\mathbf{s}_{i,j}^{\text{reg}}$ to the origin for any $i = j \pmod{2}$. It should be noted that,

$$\lim_{\Delta \rightarrow 0} D_{2i,2j}^{\text{reg}}(\Delta) = \lim_{\Delta \rightarrow 0} D_{2i+1,2j+1}^{\text{reg}}(\Delta) = h, \quad (69)$$

and

$$\lim_{\Delta \rightarrow 0} \theta_{2i,2j}^{\text{reg}}(\Delta) = \lim_{\Delta \rightarrow 0} \theta_{2i+1,2j+1}^{\text{reg}}(\Delta) = 0. \quad (70)$$

Thus, it is evident that

$$\lim_{\Delta \rightarrow 0} \eta(\text{psd}_{\max}, \Delta) = \infty. \quad (71)$$

Then, by L'Hôpital's rule,

$$\begin{aligned} \lim_{\Delta \rightarrow 0} R^{\text{reg}}(\text{psd}_{\max}, \Delta) &= \lim_{\Delta \rightarrow 0} \frac{\log_2 \left(1 + \frac{\gamma(\text{psd}_{\max})}{\eta(\text{psd}_{\max}, \Delta) + 1} \right)}{\Delta^2 \sqrt{3}/2} \\ &= \lim_{\Delta \rightarrow 0} \left(\frac{-\gamma(\text{psd}_{\max}) \eta'(\text{psd}_{\max}, \Delta)}{\Delta \sqrt{3} \log 2 (\eta(\text{psd}_{\max}, \Delta) + 1)^2} \frac{1}{1 + \frac{\gamma(\text{psd}_{\max})}{\eta(\text{psd}_{\max}, \Delta) + 1}} \right), \end{aligned} \quad (72)$$

where $\eta'(\text{psd}_{\max}, \Delta)$ denotes the first derivative of $\eta(\text{psd}_{\max}, \Delta)$ with respect to Δ . Since we have

$$\lim_{\Delta \rightarrow 0} \frac{\eta(\text{psd}_{\max}, \Delta) + 1}{\gamma(\text{psd}_{\max}) + \eta(\text{psd}_{\max}, \Delta) + 1} = 1, \quad (73)$$

to show boundedness of $\lim_{\Delta \rightarrow 0} R^{\text{reg}}(\text{psd}_{\max}, \Delta)$, it is sufficient to prove the following limit

$$\lim_{\Delta \rightarrow 0} \frac{\eta'(\text{psd}_{\max}, \Delta)}{\Delta (\eta(\text{psd}_{\max}, \Delta) + 1)^2} \quad (74)$$

is bounded. By L'Hôpital's rule, one can see that

$$\lim_{\Delta \rightarrow 0} \frac{\eta'(\text{psd}_{\max}, \Delta)}{\Delta (\eta(\text{psd}_{\max}, \Delta) + 1)^2} = \lim_{\Delta \rightarrow 0} \frac{-2}{(\eta(\text{psd}_{\max}, \Delta) + 1) \Delta^2} \quad (75)$$

Thus, if we can prove that

$$\lim_{\Delta \rightarrow 0} \eta(\text{psd}_{\max}, \Delta) \Delta^2 > 0, \quad (76)$$

we are done.

For any given $\epsilon > 0$, let $\tilde{D} > 0$ be such that the aggregate interference at $(0, 0)$ due to the satellites having distance larger than \tilde{D} is less than ϵ . There is always such \tilde{D} , because we know $\sum_n n^{-\alpha}$ is a convergent series for $\alpha > 1$. Clearly, the value of \tilde{D} depends on the beamwidths of the satellites and ground users. Accordingly, let $D \triangleq \sqrt{\tilde{D}^2 - h^2}$.

Let us define I_0 and I_1 as follows

$$I_0 \triangleq \frac{\text{psd}_{\max}}{\sigma^2} \sum_{(i,j) \neq (0,0)} (D_{2i,2j}^{\text{reg}}(\Delta))^{-\alpha} W(\theta_{2i,2j}^{\text{reg}}(\Delta)), \quad (77)$$

$$I_1 \triangleq \frac{\text{psd}_{\max}}{\sigma^2} \sum_{(i,j)} (D_{2i+1,2j+1}^{\text{reg}}(\Delta))^{-\alpha} W(\theta_{2i+1,2j+1}^{\text{reg}}(\Delta)). \quad (78)$$

It is clear that $\eta(\text{psd}_{\max}, \Delta) = I_0 + I_1$. If $(2i, 2j)^{\text{th}}$ link is leading a non-negligible interference at the ground user located $(0, 0)$, then we must have

$$i^2 + 3j^2 \leq \frac{D^2}{\Delta^2} \text{ and } (i, j) \neq (0, 0). \quad (79)$$

The number of such links, T_0 , can be easily lower bounded as

$$T_0 = \sum_{i=0}^T 2 \left\lfloor \sqrt{\frac{T^2 - i^2}{3}} \right\rfloor - 1 \quad (80)$$

$$\geq \frac{2}{\sqrt{3}} \sum_{i=0}^T \sqrt{T^2 - i^2} - (2T + 1)$$

$$\geq \frac{2}{\sqrt{3}} \int_0^T \sqrt{T^2 - x^2} dx - (2T + 1) \quad (81)$$

$$= \frac{2\pi}{4\sqrt{3}} T^2 - (2T + 1), \quad (82)$$

where $T = D/\Delta$. Via similar steps, the number of links, T_1 , causing a non-negligible interference term in the summation I_1 , can be lower bounded by the same number.

Let us denote \tilde{I} as the interference term obtained when the distance between the satellite and the ground user is equal to \tilde{D} . Thus, we can write that

$$\eta(\text{psd}_{\max}, \Delta) \Delta^2 > \frac{\pi T^2 \Delta^2}{\sqrt{3}} \tilde{I} - (4T + 2) \tilde{I} \Delta^2 \quad (83)$$

$$= \frac{\pi D^2}{\sqrt{3}} \tilde{I} - \tilde{I} (4D\Delta + 2\Delta^2). \quad (84)$$

In other words, we show that

$$\lim_{\Delta \rightarrow 0} \eta(\text{psd}_{\max}, \Delta) \Delta^2 > \frac{\pi D^2}{\sqrt{3}} \tilde{I} > 0. \quad (85)$$

Hence, we are done. \square

REFERENCES

- [1] K. T. Li, C. A. Hofmann, H. Reder, and A. Knopp, "A techno-economic assessment and tradespace exploration of low earth orbit mega-constellations," *IEEE Communications Magazine*, vol. 61, no. 2, pp. 24–30, 2022.
- [2] A. I. Perez-Neira, M. A. Vazquez, M. B. Shankar, S. Maleki, and S. Chatzinotas, "Signal processing for high-throughput satellites: Challenges in new interference-limited scenarios," *IEEE Signal Processing Magazine*, vol. 36, no. 4, pp. 112–131, 2019.
- [3] Z. Qu, G. Zhang, H. Cao, and J. Xie, "LEO satellite constellation for internet of things," *IEEE Access*, vol. 5, pp. 18 391–18 401, 2017.
- [4] S. Liu, Z. Gao, Y. Wu, D. W. Kwan Ng, X. Gao, K.-K. Wong, S. Chatzinotas, and B. Ottersten, "LEO satellite constellations for 5G and beyond: How will they reshape vertical domains?" *IEEE Communications Magazine*, vol. 59, no. 7, pp. 30–36, 2021.
- [5] A. A. Kriezis and W. Q. Lohmeyer, "U.S. market access authorization timeline analysis for megaconstellation networks," *Olin Satellite + Spectrum Technology Policy Group (OSSTP) Olin College of Engineering*, 2022.
- [6] R. A. Berry, P. Bustamante, D. Guo, T. W. Hazlett, M. L. Honig, W. Lohmeyer, I. Murtazashvili, S. Palo, and M. B. H. Weiss, "Spectrum rights in outer space: Interference management for low Earth orbit (LEO) broadband constellations," *Journal of Information Policy*, to appear. Available at SSRN 4178793, 2024.
- [7] T. Hazlett, D. Guo, and M. Honig, "From 'open skies' to traffic jams in 12 GHz: A short history of satellite radio spectrum," *Journal of Law & Innovation*, vol. 6, no. 1, pp. 66–94, 2023.
- [8] J. G. Andrews, F. Baccelli, and R. K. Ganti, "A tractable approach to coverage and rate in cellular networks," *IEEE Transactions on Communications*, vol. 59, no. 11, pp. 3122–3134, 2011.
- [9] A. Ganz, Y. Gong, and B. Li, "Performance study of low earth-orbit satellite systems," *IEEE Transactions on Communications*, vol. 42, no. 234, pp. 1866–1871, 1994.
- [10] F. Vatalaro, G. Corazza, C. Caini, and C. Ferrarelli, "Analysis of LEO, MEO, and GEO global mobile satellite systems in the presence of interference and fading," *IEEE Journal on Selected Areas in Communications*, vol. 13, no. 2, pp. 291–300, 1995.
- [11] A. Mokhtar and M. Azizoglu, "On the downlink throughput of a broadband LEO satellite network with hopping beams," *IEEE Communications Letters*, vol. 4, no. 12, pp. 390–393, 2000.
- [12] H. Mourad, A. Al-Bassiouni, S. Emam, and E. Al-Hussaini, "Generalized performance evaluation of low earth orbit satellite systems," *IEEE Communications Letters*, vol. 5, no. 10, pp. 405–407, 2001.
- [13] A. Yastrebova, I. Angervuori, N. Okati, M. Vehkaperä, M. Höyhty, R. Wichman, and T. Riihonen, "Theoretical and simulation-based analysis of terrestrial interference to LEO satellite uplinks," in *GLOBECOM 2020 - 2020 IEEE Global Communications Conference*, 2020, pp. 1–6.
- [14] N. Okati, T. Riihonen, D. Korpi, I. Angervuori, and R. Wichman, "Downlink coverage and rate analysis of low earth orbit satellite constellations using stochastic geometry," *IEEE Transactions on Communications*, vol. 68, no. 8, pp. 5120–5134, 2020.
- [15] A. Al-Hourani, "An analytic approach for modeling the coverage performance of dense satellite networks," *IEEE Wireless Communications Letters*, vol. 10, no. 4, pp. 897–901, 2021.
- [16] J. Park, J. Choi, and N. Lee, "A tractable approach to coverage analysis in downlink satellite networks," *IEEE Transactions on Wireless Communications*, pp. 1–1, 2022.
- [17] A. Talgat, M. A. Kishk, and M.-S. Alouini, "Stochastic geometry-based analysis of LEO satellite communication systems," *IEEE Communications Letters*, vol. 25, no. 8, pp. 2458–2462, 2021.
- [18] D.-H. Jung, J.-G. Ryu, W.-J. Byun, and J. Choi, "Performance analysis of satellite communication system under the shadowed-rician fading: A stochastic geometry approach," *IEEE Transactions on Communications*, vol. 70, no. 4, pp. 2707–2721, 2022.
- [19] H. Jia, C. Jiang, L. Kuang, and J. Lu, "An analytic approach for modeling uplink performance of mega constellations," *IEEE Transactions on Vehicular Technology*, pp. 1–11, 2022.
- [20] N. Okati and T. Riihonen, "Nonhomogeneous stochastic geometry analysis of massive LEO communication constellations," *IEEE Transactions on Communications*, vol. 70, no. 3, pp. 1848–1860, 2022.
- [21] H. W. Kuhn, "The hungarian method for the assignment problem," *Naval Research Logistics Quarterly*, vol. 2, no. 1-2, pp. 83–97, 1955. [Online]. Available: <https://onlinelibrary.wiley.com/doi/abs/10.1002/nav.3800020109>
- [22] 3GPP, "Study on New Radio (NR) to support non-terrestrial networks," 3rd Generation Partnership Project (3GPP), Technical Specification (TS) 38.811, 10 2020, version 15.4.0.
- [23] E. Kim, I. P. Roberts, and J. G. Andrews, "Downlink analysis and evaluation of multi-beam LEO satellite communication in shadowed rician channels," 2022. [Online]. Available: <https://arxiv.org/abs/2207.06663>
- [24] R. Wang, M. A. Kishk, and M.-S. Alouini, "Evaluating the accuracy of stochastic geometry based models for LEO satellite networks analysis," *IEEE Communications Letters*, vol. 26, no. 10, pp. 2440–2444, 2022.
- [25] A. Abdi, W. Lau, M.-S. Alouini, and M. Kaveh, "A new simple model for land mobile satellite channels: first- and second-order statistics," *IEEE Transactions on Wireless Communications*, vol. 2, no. 3, pp. 519–528, 2003.